

## RESEARCH ARTICLE

# Large eddy simulation of passive noise reduction in subsonic jets by using chevrons

K. Tewari<sup>1\*</sup>, A. Dewan<sup>1</sup>, V. Narayanan<sup>2</sup>, G. Dogra<sup>3</sup><sup>1</sup> Department of Applied Mechanics, Indian Institute of Technology Delhi, 110016, New Delhi, India  
Phone: +91-8410410277<sup>2</sup> Department of Mechanical Engineering, Indian Institute of Technology Gandhinagar, 382055, Gujarat, India<sup>3</sup> School of Interdisciplinary Research, Indian Institute of Technology Delhi, 110016, New Delhi, India

**ABSTRACT** - Chevrons are widely used passive noise reduction devices that have emerged as a significant breakthrough for aircraft industry in enabling substantial noise reduction without sacrificing thrust. However, the conventional testing of different chevron designs necessitates costly experimental facilities. This challenge can be circumvented through computational validation using computational fluid dynamics (CFD). Hence, this study employs a hybrid computational aeroacoustics approach to assess the viability of chevrons as a passive noise reduction technique within free subsonic jets using the commercial CFD software. Two sets of numerical simulations performed with and without chevrons applied at the end of the nozzle were examined. The dynamic Smagorinsky model was utilized to resolve the sub-grid scale stresses in these simulations of turbulent flows, which were run using large eddy simulation at an exit Mach number of 0.75. Using Ffowcs Williams Hawkins acoustic equations and the Fourier transform, the far-field analysis was performed on the acquired flow field to calculate the jet noise distribution in terms of the Sound Pressure Levels. The simulation results for free jets show good agreement with the published experimental data in terms of capturing the mean flow field and the acoustic levels in farfield. The simulations with chevrons show a reduction of approximately 2-3 dB in the farfield which results from a reduction in low-frequency mixing noise due to the creation of vortices in the shear layers. This result substantiates the capability of the computational aeroacoustics technique to evaluate chevron designs for effectively mitigating jet noise, particularly at high Mach numbers.

**ARTICLE HISTORY**Received : 09<sup>th</sup> Sept. 2023Revised : 23<sup>rd</sup> Apr. 2024Accepted : 16<sup>th</sup> June 2024Published : 28<sup>th</sup> June 2024**KEYWORDS***Large eddy simulation**Jet noise**Chevrons**FW-H method**Sound pressure level*

## 1. INTRODUCTION

With the requirement of faster modes of transportation systems and global reduction in jet fuel prices, air travel has become a reliable mode of transport. Every year, the aviation industry experiences a substantial rise in the number of passengers, which has led to the demand for further expansion, as reported by statistics published in various studies [1, 2]. Although this expansion has improved the connectivity between places by reducing the time of travel, at the same time, it has also become a severe cause of concern for the people living near the airports due to the associated heavy noise emissions, as pointed out by Basner et al. [3]. The emitted noise from aircraft not only affects the social life of residents, but its prolonged exposure could lead to diseases, such as, hypertension, psychological disorders, and even Noise-Induced Hearing Loss, as highlighted by Kaltenbach et al. [4]. Hence, attempts to mitigate noise started as soon as the aircraft industry expanded and became commercial. As highlighted in past studies [5–7], multiple noise sources are present in an aircraft, such as, fan, jet, turbine, combustor, and compressor. Besides these, the aircraft frames, and other moving parts, such as, flap side edges, landing gear, wingtip, and trailing edge, also contribute to the aircraft noise. Jet noise has been found to contribute significantly to the total noise emissions; as a result, any reduction in jet noise has a considerable impact on the total noise emissions.

Primary sources of noise in jet encompass diverse mechanisms. These include shock interactions, known to yield shock-associated noise, resonant phenomena at the tip generating transonic tones, impinging tones, and screech, as well as the interplay between the jet and the surrounding free stream. Among these various jet noise sources, the primary source of noise in most jets used in commercial aircraft that fly at subsonic speed these days is noted to be the interaction of the jet fluid with the ambient free-stream fluid [8–10]. This mixing of the high-velocity jet stream with the ambient quiescent air results in significant large-scale and fine-scale turbulence structures, which generate noise. This aerodynamically generated jet noise gets advected further downstream by the interaction of eddies with the mean flow. This dynamic interplay imparts a distinct directional characteristic to the noise sources, with the mean flow predominantly conveying the bulk of sound energy in the downstream direction, as mentioned in previous studies [8, 11]. Since the noise sources are formed beyond the engine exhaust due to the interaction of the shear layers, corrective action needs to be applied in this area to reduce noise levels. This concept has led to the development of many noise reduction techniques

\*CORRESPONDING AUTHOR | K. Tewari | ✉ [kamal.tewari1@email.com](mailto:kamal.tewari1@email.com)

aimed at modifying the flow at the exit. One such technique was using bypass streams in turbofan engines, as suggested by Dimitri [12]. Although this technique proved successful in suppressing the overall noise levels due to a reduction in the jet velocity, the maximum reduction in the noise levels was limited by the maximum bypass ratio. Subsequent studies [13–17] explored a range of novel techniques, such as, swirling the flow in the exit of the nozzle, using acoustic absorbers such as liners at the end, and active noise cancellation techniques but some of these were limited by their impact on engine thrust. In 1996, NASA tested a new noise reduction method by modifying the trailing edge of the jet to have chevrons. This approach aimed to reduce the noise levels by mixing the core and bypass flows in the case of turbofan engines or by mixing the potential core with the ambient stream in the case of turbojet engines. It proved to be the first successful test where the jet noise concept did not have a serious impact on thrust, and the thrust loss was limited to a marginal value [18]. This milestone opened up fresh avenues for researchers to delve into the optimization of chevron configurations encompassing shapes, sizes, and quantities [18–22]. However, for successful optimization of these parameters, one requires validation against a variety of test cases, which in turn demands expensive experimental facilities and time.

Computational Fluid Dynamics (CFD) tools, complemented by sophisticated techniques for analyzing intricate turbulent flows like Direct Numerical Simulation, Large Eddy Simulation (LES), have emerged as compelling alternatives to drive pioneering advancements in this domain. Historically, CFD tools have been predominantly applied to investigate fluid flow within a multitude of contexts. These encompass a broad spectrum of applications, including the examination of phenomena like jet impingement, the dynamics of fluid within pipes, and the expansion characteristics of jets emerging from nozzles, among various others as reported in the literature [23–27]. Recently these tools coupled with the numerical acoustic solvers have become popular to model the noise generation and have led to the development of a new branch known as computational aeroacoustics (CAA), which provide a practical avenue for advancement, especially in cases where extensive experimental resources are not accessible. The pioneering work to numerically model the jet noise was carried out by Lighthill [28]. Since then, this field has advanced significantly by contributions from researchers, such as, Ffowcs Williams and Hawkings [29], Goldstein [30, 31], etc. In recent years, improvements in computational facilities and numerical techniques have accelerated the developments in this field and have made the hybrid numerical approach using integral methods coupled with unstructured grid CFD solvers quite popular. The use of these hybrid techniques, in which the nearfield acoustic field is resolved using CFD and the wave solution is then extended to the far field observer location, has accelerated research on jet noise estimation by significantly bringing down the computational cost, as shown in past studies [32–34]. These hybrid strategies have been used in past research [35–37] to predict the far-field noise from an expanding free jet. Bres and Lele [38] present a thorough assessment of the literature on the different high-fidelity turbulence techniques, including LES and Hybrid LES, that have been applied to estimate jet noise under a variety of flow conditions. However, very few studies in the literature have evaluated the LES approach to simulate noise emission from subsonic turbulent jets by systematically validating the results against experiments, particularly for the high Mach number subsonic jet flow.

The objective of the present work is therefore to assess the effectiveness of the CAA in predicting noise emissions from high Mach number subsonic jet and to understand the impact of chevrons on flowfield and noise emissions. This investigation seeks to enhance our understanding of chevrons as a passive noise reduction device and to evaluate CAA as a cost-effective alternative to traditional experimental methods for high Mach number flows. A subsonic turbulent jet with a Mach number of 0.75 emerging from a circular nozzle is analyzed. LES initialized from Reynolds-Averaged Navier-Stokes (RANS) computations is employed to resolve the large-scale features of the flow field, which are known to be primarily responsible for noise generation [39]. For modeling the fine scales of the flow field, the dynamic Smagorinsky subgrid-scale model has been used, and the far-field acoustic field was computed using Ffowcs Williams Hawkings (FW-H) acoustic equations. The various parameters studied are the jet entrainment rate, turbulent and mean velocity profiles, sound pressure level, etc., which provide a comprehensive description of the flow field. The results of the baseline simulations have been validated against the experimental work of Jordan et al. [40] for the same operating conditions. The results obtained by applying chevrons at the exit of the nozzle for the same exit Mach number show an appreciable reduction in the noise levels, which justifies their usage in jet engines.

## 2. MATERIALS AND METHODS

To investigate the efficacy of chevrons for jet noise reduction, two sets of simulations with different nozzle configurations (with and without chevrons) were run at a Mach number of 0.75. Table 1 lists the operating conditions for the two scenarios, with the first case corresponding to the attributes of a baseline nozzle and the second case to those of a nozzle with chevrons at the exit.

Table 1. Operating conditions used in the simulations

S. No.	$U_j/c$	$M_i$	$M_\infty$	TR	$Re_j$	$P_i$
1	0.75	0.16	0.006	1	50000	44800 Pa
2	0.75	0.20	0.006	1	50000	44800 Pa

In Table 1, the subscript  $i$  represents the reservoir state at the nozzle's entrance, whereas subscript  $j$  and  $\infty$  represent the values of the variables inside the jet and free-stream conditions, respectively. The jet considered in both cases is assumed to be an isothermal jet ( $T_j/T = 1.0$ ), and the nozzle walls are considered adiabatic. For all the cases, the Mach

number at the exit of the jet is kept constant at  $M_j = 0.75$ , which, based on the nozzle's exit diameter, corresponds to the Reynolds number ( $Re$ ) of  $1 \times 10^5$ . Though this value of  $Re$  is lower than the experimental value, it has been found to be satisfactory in capturing all the significant noise effects in the previous work [33]. It is based on the observation that when the value of  $Re$  exceeds  $1.0 \times 10^5$ , the behaviour of a jet becomes independent of its initial conditions [41]. The far-field noise was computed from the obtained LES results by applying the FW-H analogy, and an open conical surface was chosen as an FW-H surface for far-field noise computation as it is an ideal choice, as reported in the literature [42].

## 2.1 Computational Domain

The nozzle dimensions, as shown in Figure 1, are the same as that of the nozzle used in the Jet Exhaust Aerodynamic Noise (JEAN) project, which had a total length of 0.38 m. The inlet diameter of the nozzle is 0.075 m, and the diameter at the exit of the nozzle is  $D_j = 0.05$  m. The length of the whole computation domain beyond the nozzle exit is taken as  $72 D_j$ , while the FW-H surface, which is a cone, extends only up to  $40 D_j$ . The radial distance of the flow domain extends from  $30 D_j$  at the far field inlet to  $50 D_j$  at the far-field outlet.

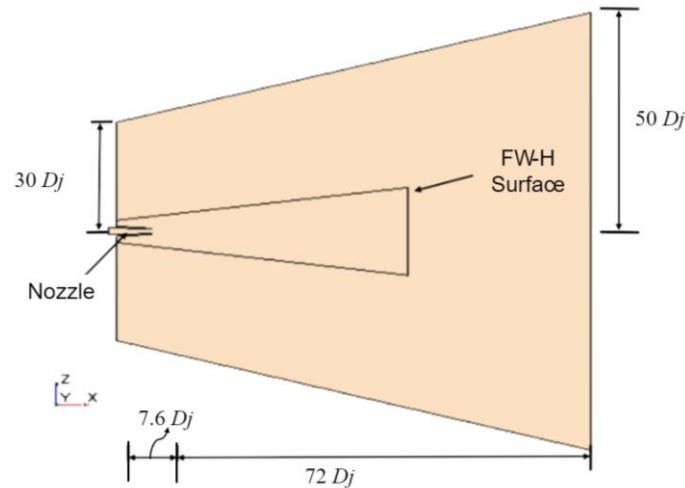


Figure 1. Dimensions of the computational domain used for free jet nozzle

For the second case, the nozzle geometry was modified slightly by introducing chevrons (eight in the total count), which were placed at its end with a penetration (the difference in radius between the base and tip of the chevron) of 0.003 m. In order to maintain the same nozzle exit Mach number in both cases, the Mach number at the entrance of the nozzles was changed using the isentropic relations. This allowed a comparison of the jet noise from the same nozzles but with different nozzle profiles at the same jet exit Mach numbers.

## 2.2 Meshing

As illustrated in Figure 2, the computational domain is characterized by a boundary-fitted unstructured mesh that can be effectively partitioned into two distinct subdomains, each serving specific accuracy needs. A finely detailed inner region adeptly captures turbulence-induced noise sources, while a relatively coarser mesh characterizes the far-field region, optimizing computational efficiency. Hexahedral cells with prism layers on the walls are strategically used to accurately represent shear layers. Notably, mesh adjustments are strategically applied along the jet flow's centerline to better encapsulate the inherent flow dynamics of the shear layers. To refine the mesh with precision, a conical refinement region is incorporated, extending towards the domain's wall boundaries. This meticulous mesh adaptation strategy contributes to an enhanced representation of flow characteristics and noise dynamics, effectively balancing computational accuracy with efficiency.

The mesh has seven volumetric refinements applied in succession to the jet nozzle exit (see Figure 2). This gradual coarsening of the mesh towards the outlet boundary helps us to ensure that no noticeable acoustic reflection is observed from the vertical waves exiting the outlet boundary. The base size was taken to be 0.025 m, and the successive refinements (as a percentage of base size) were made as shown towards the nozzle. For the nozzle, the mesh includes five prism layers, each adhering to a stretching factor of 1.3. This configuration ensures the accurate depiction of boundary shear layers, which is essential for capturing the flow's intricacies. Based on the convergence tests carried out using the centreline velocity of the jet as a reference, a mesh size of 23 million was chosen.

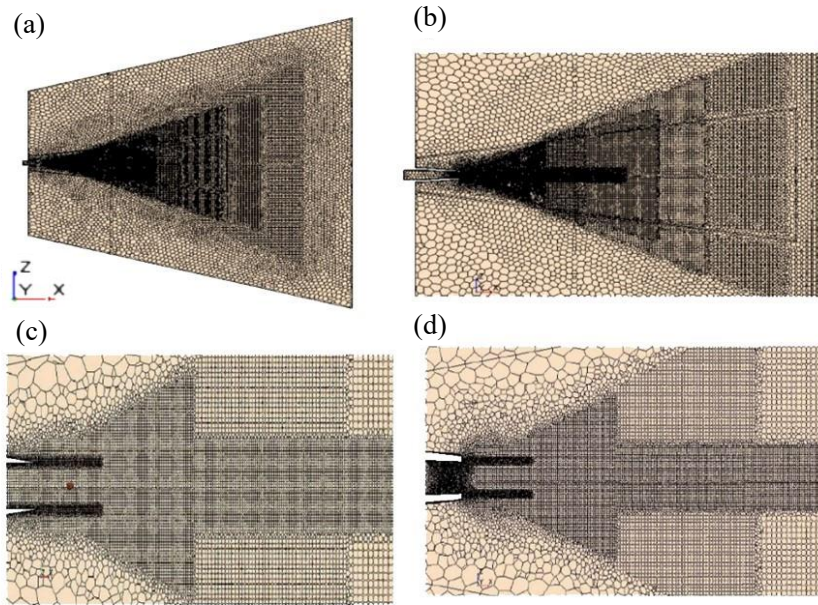


Figure 2. (a) Mesh details showcasing successive refinements near the nozzle exit, (b) close-up view, (c-d) close-up view of the mesh domain used near the nozzle exit for cases without and with chevrons, respectively

### 2.3 Boundary Conditions

The nozzle walls were subject to a no-slip wall boundary condition, accompanied by adiabatic thermal conditions. The exit of the domain was treated as a pressure outlet. All the other domain boundaries were treated as the free-stream boundaries with pressure  $P_\infty = 99670$  Pa and Mach number  $M_\infty = 0.006$  to model the free jet flow. The stagnation pressure and temperature values were specified at the inlet as  $P_0 = 144470$  Pa and  $T_0 = 315$  K and the turbulence intensity of 5% was prescribed. The acoustic suppression zone model was used on the external free-stream boundary to add appropriate damping source terms and avoid reflection.

### 2.4 LES and FW-H Solver

Large Eddy Simulation is a transient simulation technique for studying turbulence in which the large scales of turbulence are solved directly while the small scales of motion are considered using sub-grid scale models [43, 44]. The idea is to compute the largest turbulent eddies down to a certain cutoff width. The smallest eddies below this cut-off width are simpler and are modelled with sub-grid scale models. This method provides better results than the Reynolds-Averaged Navier-Stokes modelling in capturing the flow details and sound emissions in 3-D unsteady turbulent flows and thus it better resolves the noise sources generating the acoustic field as demonstrated in the past studies [35, 45–47]. LES make use of filtering in the governing Navier-Stokes equations instead of time averaging in the RANS equations and filters out the eddies associated with small length scales (i.e., high frequency) than the cut off frequency. The spatial filtering function in LES is given by the expression:

$$\overline{\Phi(x, t)} = \int_{-\infty}^{\infty} \int_{-\infty}^{\infty} \int_{-\infty}^{\infty} G(x, x', \Delta) \phi(x', t) dx'_1 dx'_2 dx'_3 \quad (1)$$

where,  $\overline{\Phi(x, t)}$  is filtered function,  $G$  is the filtering function and  $\Delta = (\Delta x \Delta y \Delta z)^{\frac{1}{3}}$  is the filter cut-off width. The filtered equations for LES on rearrangement look similar to the unsteady RANS equations (see Shukla and Dewan [46]) with the difference in the turbulence stress tensor which is given by the expression:

$$B = 2\mu_t S - \frac{2}{3} (\mu_t \nabla \cdot u + \rho k) I \quad (2)$$

where,  $\mu_t$  and  $k$  are the subgrid scale turbulent viscosity and kinetic energy, respectively.  $S$  is the strain rate tensor calculated from the resolved velocity field in this instance as:

$$S = \frac{1}{2} (\nabla u + \nabla u^T) \quad (3)$$

The turbulent viscosity within the model simulations is modelled using the Dynamic Smagorinsky model which uses the mixing length hypothesis for modelling the subgrid-scale stresses, as discussed in Meneveau et al. [48]. The sub-grid scale kinetic energy in this model which is used to determine the subgrid scale kinematic viscosity is calculated algebraically by assuming the condition of the local equilibrium. The Ffowcs Williams and Hawkins [29] method used in the present work for the far-field noise computation is basically a surface integral method that relies on the near-field details about the sound source obtained from the near-field flow data using a CFD solution. The generalised wave

equation's analytical solution is used to calculate the propagation of sound in the FW-H method rather than doing an explicit calculation. Hence, unlike previous numerical techniques like the Lighthill analogy or Goldstein's generalised acoustic analogy, any acoustic information is not lost. The sound propagation into the free space is determined here without including the effects, such as, sound reflections, refraction, or changes in material properties. The equation used is basically an inhomogeneous wave equation and it requires time accurate data in the near-field flow for the noise source information. The following wave equation can be used to illustrate the FW-H equation:

$$\frac{1}{a_0^2} \frac{\partial^2 p'}{\partial t^2} - \nabla^2 p' = \frac{\partial^2}{\partial x_i \partial x_j} \{T_{ij} H(f)\} - \frac{\partial}{\partial x_i} \{[P_{ij} + \rho u_i (u_n - v_n)] \delta(f)\} + \frac{\partial}{\partial t} \{[\rho_0 v_n + \rho (u_n - v_n)] \delta(f)\} \quad (4)$$

where,  $u_i$  denotes the component of the fluid velocity in the  $x_i$  direction,  $u_n$  is the component of the velocity normal to the surface,  $v_i$  is component of the surface velocity in the  $x_i$  direction, and  $H(f)$  and  $\delta(f)$  are the Heaviside and Dirac delta functions, respectively. In the equation  $p'$  is the sound pressure at the far field and  $T_{ij} = \rho u_i u_j + P_{ij} - a_0^2 (\rho - \rho_0) \delta_{ij}$ . The general solution to this equation using the Green's function is given by:

$$p'(x, t) = p'_T(x, t) + p'_L(x, t) \quad (5)$$

$$4\pi p'_T(x, t) = \int_{f=0} \left[ \frac{\rho_0 (\dot{U}_n + U_n)}{r(1 - M_r)^2} \right] dS + \int_{f=0} \left[ \frac{\rho_0 U_n \{rM_r + a_0(M_r - M^2)\}}{r^2(1 - M_r)^3} \right] dS \quad (6)$$

$$4\pi p'_L(x, t) = \frac{1}{a_0} \int_{f=0} \left[ \frac{L_r}{r(1 - M_r)^2} \right] dS + \int_{f=0} \left[ \frac{L_r - L_m}{r^2(1 - M_r)^2} \right] dS + \int_{f=0} \left[ \frac{L_r \{rM_r + a_0(M_r - M^2)\}}{r^2(1 - M_r)^3} \right] dS \quad (7)$$

where, the term  $p'_T(x, t)$  represents the thickness noise which is generated due to the displacement in volume of the fluid  $L_i = P_{ij} n_i + \rho u_i (u_n - v_n)$  and the other term  $p'_L(x, t)$  is the loading noise which occurs due to the fluctuating force fields. In the above equation,  $\rho$  is far field density and  $M$  denotes the surface Mach number. The quad pole volumetric noise source's source locations are defined by the FW-H surfaces, and an impermeable FW-H surface serves as a filter for the wall boundary conditions where noise originates. It ignores the contribution from the volumetric sources located outside of this impermeable surface and only considers the noise emission from sources that are present inside the surface.

### 2.5 Modelling Details

The large eddy simulations were started from an initially converged RANS computation in which the working fluid was assumed to be an ideal gas. This approach allows the excitation of the shear layer in the absence of any forcing parameter, as outlined by Shur et al. [49]. The governing equations were solved using the implicit unsteady solver in which the temporal scheme was chosen to be second-order accurate. The simulation progressed with a time step of  $2.0 \times 10^{-5}$  seconds after each iteration. The Bounded Central Differencing scheme) was used in the segregated flow solver to calculate the convective fluxes. The convective temperature flux calculation scheme was the Monotonic Upstream-centered Scheme for Conservation Laws (MUSCL), which is a third-order accurate with an upward blending factor of 0.15. The dynamic Smagorinsky model, in which the Smagorinsky constant varies in location and time, was employed to resolve the sub-grid scales. The far-field acoustic zone at various locations was predicted using the FW-H approach after the mean-field profiles were generated at a frequency of 200-time steps. The flow averaging and sampling were then started after 0.02 seconds when the solutions converged.

## 3. RESULTS AND DISCUSSION

The flow field results and the noise emissions from the jets by the two nozzle configurations (i.e., without and with chevrons) at a subsonic speed are discussed in this section. First, the validation of important mean flow parameters with the reported experimental results by Jordan et al. [40] are presented in Section 3.1. Subsequently the results by applying chevrons in the nozzle are discussed briefly in Section 3.2.

### 3.1 Nozzle without Chevron

The jet flow discharged from the nozzle without chevrons exemplifies a scenario of a turbulent free jet, where the mean flow gradients evolve without encountering confining boundaries. Figure 3 shows the instantaneous velocity profile in the free jet formed from the nozzle. It can be seen that as the flow leaves the nozzle at high speeds, it tries to pierce the stationary ambient air stream. This results in velocity gradients in the flow field and the formation of shear layers. As the jet develops, it becomes turbulent and can be distinguished from the non-turbulent surrounding fluid by a super viscous layer, whose boundary changes continuously. However, the initial shear layer at the nozzle exit remains more or less undisturbed. These large-scale turbulence structures produced in the downstream region of the jet also serve as a noise source that spreads in the far-field area.

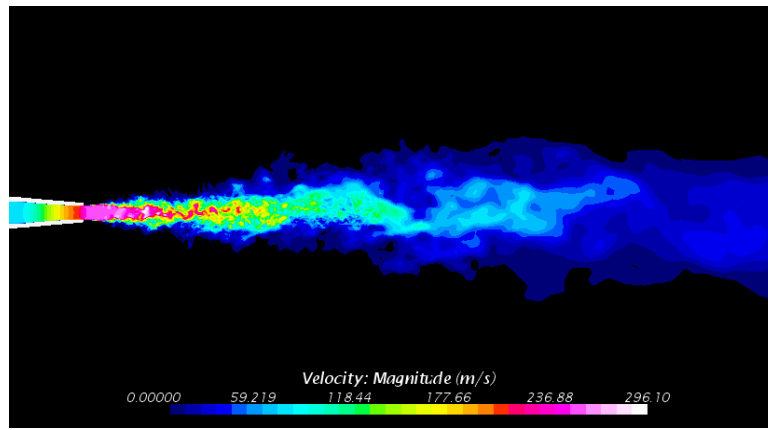


Figure 3. Contours of the instantaneous velocity field of the simulated free jet

Figure 4 shows the mean profile of the jet in which different regions of the free jet can be distinguished. The boundaries of the shear layers that separate the jet from the ambient fluid are visible, and they grow continuously as the jet develops. In the downstream region, as the jet develops it entrains the surrounding fluid and adopts a conical shape, as in the case of symmetrical jets. Therefore, the shear-layer boundary is seen to be continuously growing downstream as the jet develops. At the same time, it can be observed that the radial extent of the potential core (a region where the mean jet velocity is approximately 0.99 times the exit velocity) is decreasing downstream, which indicates that the increase in turbulence in the flow enhances mixing in the downstream region. It can also be observed that the gradients in the radial direction are much larger due to a rapid mixing than in the flow direction, which is also clear from the radial and axial velocity profiles of the jet, as discussed below.

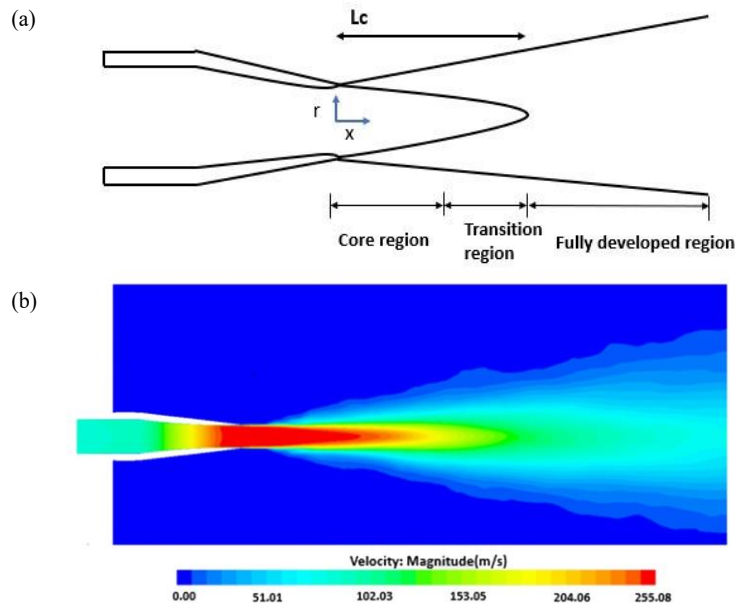


Figure 4. Schematic representation of jet flow field and contours of mean velocity profile in x-z plane showing different regions of the jet

Figure 5 shows the axial variation in the normalized jet velocity along the center line obtained from the simulation and its comparison with the reported experimental data [40] and various other past simulation studies [50, 51]. The fully developed region of the jet is approximately at  $x = 4.0 D_j$ , which matches quite well with the experimental results despite slight underprediction in the jet velocity at a larger distance, likely due to the relatively coarser mesh used downstream. The results obtained by LES with the dynamic Smagorinsky sub-grid scale model also better capture the axial velocity variation compared to the previous model studies.

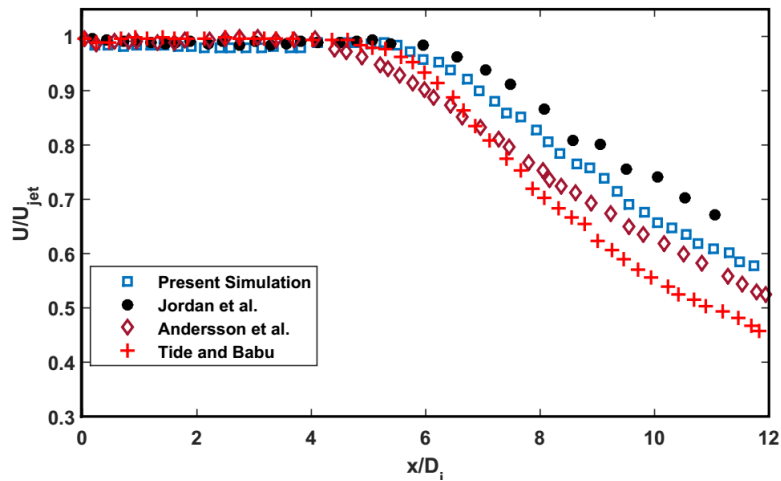


Figure 5. Profiles of the normalized center line velocity at different location along its central line and comparison with the reported experimental and numerical studies

The radial velocity profiles at three different axial locations, i.e., at  $1.0 D_j$ ,  $2.5 D_j$ , and  $5.0 D_j$ , are shown in Figure 6, which clearly shows the breaking up of the jet potential core region in the downstream direction. The radius of the potential core of the jet is, in general proportional to the axial distance downstream from the exit of the nozzle. From these profiles, it can also be observed that the gradient in the radial direction initially is quite large, and as the jet expands downstream due to mass entrainment, the gradient becomes relatively smooth. The agreement between the simulated profile and the experimental results suggests that the LES successfully and satisfactorily captures the mean velocity variations within the jet.

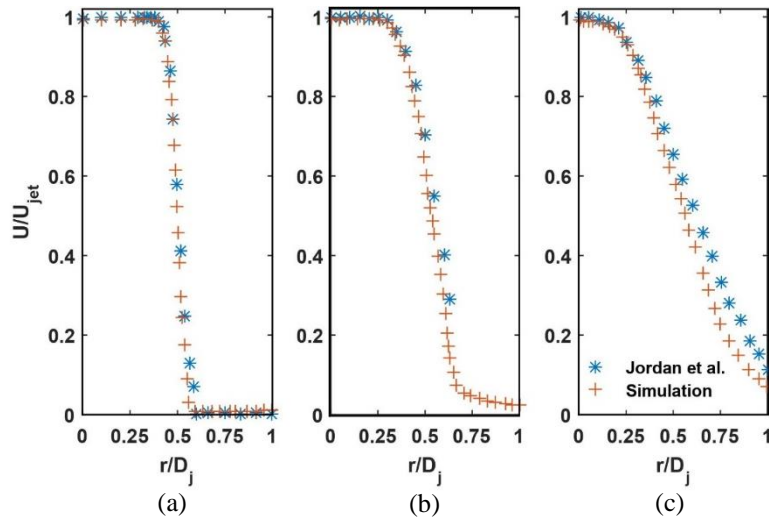


Figure 6. Normalized radial velocity profiles at different axial location: (a)  $1.0 D_j$ , (b)  $2.5 D_j$ , and (c)  $5.0 D_j$  and their comparisons with the reported experimental results

The acoustic characteristics of the simulated flow field were studied by making far-field noise measurements at a distance of  $30 D_j$  from the nozzle’s exit at various angles, as shown in Figure 7. The results obtained from the analysis were also compared with the levels reported by Jordan et al. [40]. To compute the acoustic fields at different receiver locations after the unsteady flow solutions from the LES computations were known, the pressure perturbations were first calculated on the acoustic data FW-H (permeable) surface surrounding the jet as suggested by Andersson et al. [50]. Thereafter, the post-processing operations were carried out to estimate the Sound Pressure Levels (SPL) at different locations using the FW-H equation.

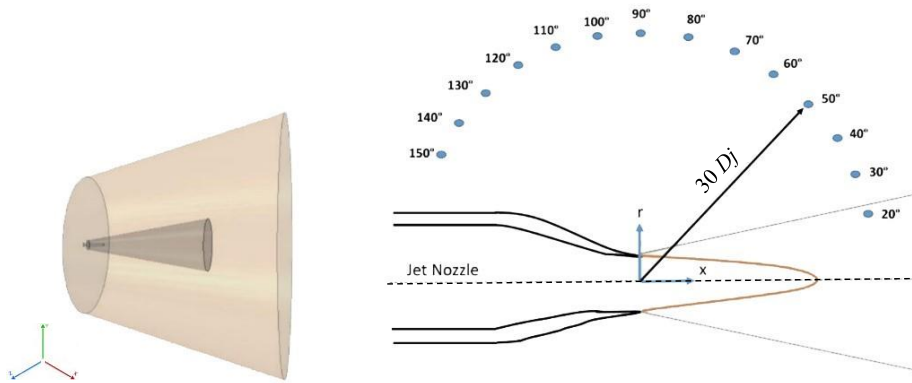


Figure 7. Locations of the FW-H receivers in the computational domain

Figure 8 shows the far-field SPL results obtained from the LES simulations. The results match with the experimental results quite accurately and are within  $\pm 3$  dB deviation at all angles. The Sound Pressure levels in Figure 8 are calculated as:

$$SPL = 20 \log_{10} \left( \frac{\sqrt{\overline{(p')^2}}}{p_{ref}} \right) \quad (8)$$

where,  $p_{ref} = 2.0 \times 10^{-5}$  Pa. These SPL results can be seen as a direct measure of Overall Sound pressure level (OASPL) as the acoustic data is band passed for a frequency of 250 to 5000 Hz. In actual practice, however, the OASPL must include all the spectral information, but this filtering is carried out to consider the absorption of both low and high frequencies in the anechoic chamber, as suggested by Andersson et al. [50].

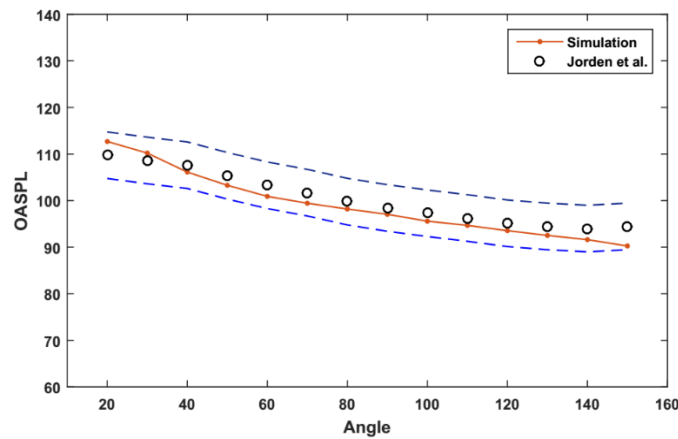


Figure 8. OASPL at different angular receivers location and its comparison with the reported experimental results

As depicted in Figure 8, the OASPL exhibits a declining trend with increasing angles of the receivers, while it becomes more pronounced at lower angles. This phenomenon can be attributed to the dynamics of a jet flow. The sound-generating entities, predominantly turbulent eddies, are transported downstream by the prevailing mean flow. Therefore, they act like a moving source of sound, and it is observed that these moving sources tend to radiate more sound in the direction in which the source is transported [29].

### 3.2 Nozzle with Chevron

A chevron is a device that is added at the exit of a nozzle (which contains saw-like structures) that protrudes into the flow field exiting from the nozzle. These devices are the current state-of-the-art techniques used for jet noise reduction in medium and high bypass turbofan engines. The serrations of the nozzle with chevrons along its trailing edge cause flow perturbation by introducing vorticity into the shear layers. This introduction of the initial vorticity acts in such a way that it enhances the mixing of jet fluid with ambient fluid and reduces the overall jet noise. The numerical results obtained in the present work by applying a total of eight such chevrons at the exit of the nozzle with a penetration (the difference in radius of the nozzle at the tip and the base of the chevron) of 0.003 m are presented in this section. The computational domain is maintained at the same size as in the primary case, along with the nozzle's length and exit diameter. It was observed that for the same inflow conditions, chevrons lowered the effective jet velocity. Therefore, the inflow conditions were slightly modified by increasing the inlet Mach number. LES was performed over the computational domain for the same exit Mach number, i.e., 0.75, and the locations of the FW-H surfaces and receivers used were kept the same for intercomparison with the baseline results.

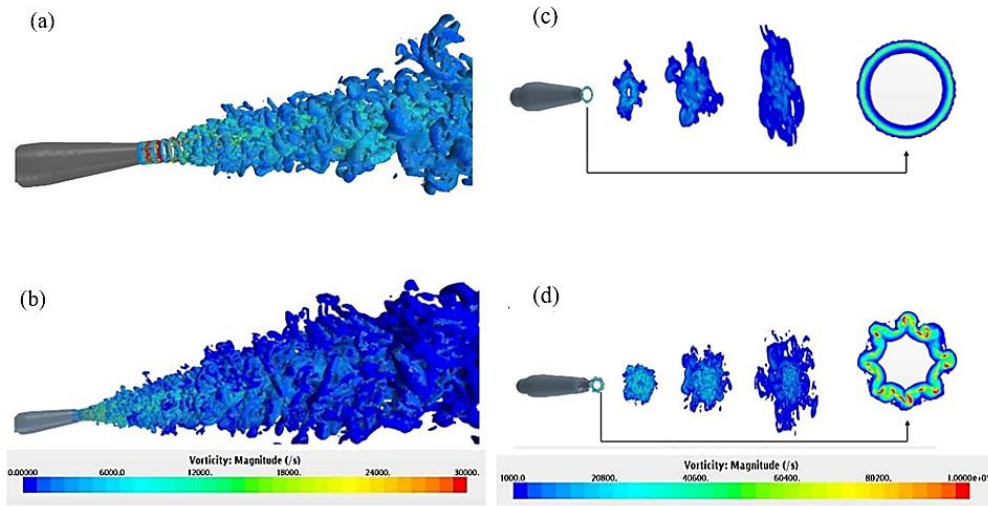


Figure 9. Vorticity isosurface of the jets: (a, b) based on Q-criteria ( $5 \times 10^5$ ) and the contours of vorticity (c, d) at different axial planes in the downstream region. (a) and (c) correspond to nozzle without chevrons and (b) and (d) correspond to nozzle with chevrons

Figure 9 shows the three-dimensional shape of the vortices near the outlet of the two nozzles. It can be seen from Figure 9(a-b) that the vortex structures of the jets emitted from the two nozzles are considerably different. Near the nozzle outlet, the base configuration displays the typical toroidal structures resulting from the Kelvin-Helmholtz instability followed by a vortex roll-up process. However, for the nozzle with chevrons, complete turbulent structures can be observed at the nozzle exit. By contrasting the vorticity profiles at different axial distances from the end of the nozzle in Figure 9(c-d), it can be observed that the axial vorticity produced by chevron nozzles near the potential core region improves cross-stream transport and results in effective mixing in the shear-layer. Vorticity is introduced into the flow as two pairs of counter-rotating vortices appear behind each edge of each individual chevron as it tries to wrap around the nozzle. The axial vorticity at its edges encourages mixing and enhances the mass entrainment rate by increasing the cross-stream transport in the shear layer. The axial propagation of this vorticity is limited because these vortices formed are counter-rotating and try to beat each other. Hence, an increase in turbulence is observed at the nozzle outlet, followed by a corresponding decrease in the jet core, which is the main noise-producing region.

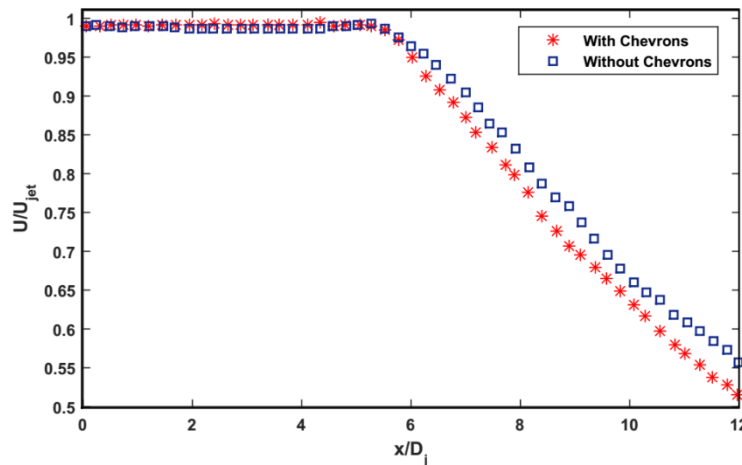


Figure 10. Comparison of the normalized center line velocity at different downstream locations for the cases with and without chevrons

A comparison of the normalized center line velocity variations for the two jets is shown in Figure 10. Despite the use of two different initial conditions, the profiles are essentially similar in both cases. However, it can be seen that the decay rate is substantially higher for the nozzle with chevron. The fully developed region for both jets is approximately  $x = 4D_j$ , but for the chevron nozzle, the mixing is enhanced, which increases the decay rate of the centreline velocity. From the RANS simulations (not shown), it was also observed that for the same initial conditions in both cases, the potential core region of a nozzle with a chevron is much smaller than that without chevrons. As the jet exits the nozzle, the amount of turbulent fluid contained in it continuously increases due to the entrainment of the surrounding fluid.

The mass flow rate can be easily computed in Star CCM+, at any axial location by simply integrating the mean axial velocity over the cross-sectional areas of a plane where the radial component of velocity is negligible, and this mass flow rate is given by the expression:

$$\dot{m} = \iint \rho U_z dx dy \tag{9}$$

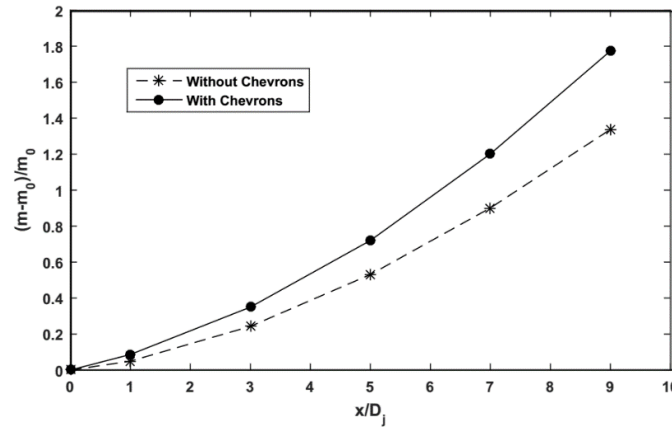


Figure 11. Comparison of the profiles of mass entrainment ratio at different locations for the cases with and without chevrons

After computing the mass flow rate, the mass entrainment ratios are then computed by the following equation:

$$\varphi = (\dot{m} - \dot{m}_0) / \dot{m}_0 \tag{10}$$

where,  $m_0$  is the mass flow rate at the nozzle exit. Figure 11 provides a visual contrast of the mass entrainment ratio across multiple cross-sections along the centerline of the jet. Notably, when considering the nozzle equipped with chevrons, an evident pattern emerges wherein the mass entrainment ratio is consistently higher across all positions. This observation underscores a more rapid rate of mixing in the downstream domain, substantiating the positive impact of chevrons on the jet's flow dynamics and mixing efficiency.

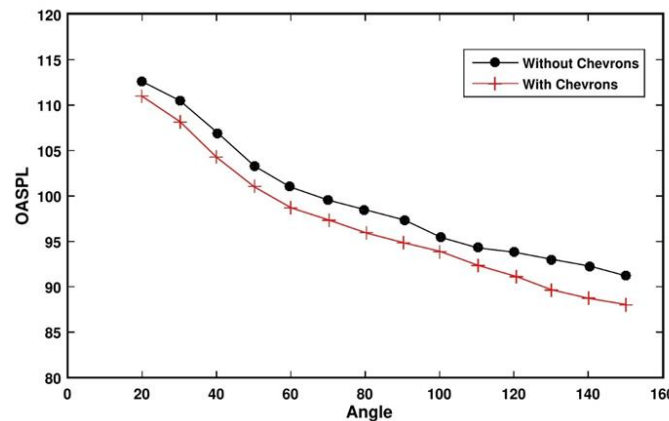


Figure 12. Comparison of the OASPL at different receivers for the cases with and without chevrons

Figure 12 shows an intercomparison of the OASPL obtained after applying the chevron against the baseline nozzle. It can be observed that the OASPL for a nozzle with a chevron is 3-4 dB lower than that without the chevrons at all angles, although the jet exit Mach number is the same. This reduction in SPL is due to a low-frequency noise reduction, as observed in various experimental studies [52]. Chevrons change the flow features at the exit of the nozzle by impinging slightly into the subsonic flow, and it causes the flow passing over its edges to turn around and thus introduce a rotational component in the flow. This, in turn, leads to a tiny counter-rotating vortex, which reduces the low-frequency noise due to the creation of finer structures. These vortices try to speed up the mixing process and have been found to bring the flow quickly to the low shear conditions.

#### 4. CONCLUSIONS

A transient three-dimensional computational study of jet noise reduction using a passive noise cancellation approach based on a chevron nozzle at the same exit Mach number was presented and discussed. The Navier-Stokes equations were computationally solved, and the effects of chevrons on the emitted noise characteristics were analyzed. The turbulent

flow field near the subsonic jet was resolved using a large eddy simulation technique, and this methodology was found suitable for predicting the mean jet characteristics, both in the radial and axial directions. The Ffowcs Williams and Hawkings equation was applied to the resolved flow fields to obtain the far-field results, and it was noted that the resolved acoustic field was in good agreement with the previously reported experimental noise emission from a single stream nozzle without chevrons. Simulations with chevrons located at the exit of the nozzle showed a considerable increase in mass entrainment and a noise reduction of approximately 2-3 dB at the far-field. This decrease happens due to the nozzle serrations reducing the low-frequency mixing noise due to the creation of vortices in the shear layers, which lowers the OASPL. Overall, the simulation findings closely align with the experimental results from literature, underscoring the viability of a hybrid approach for predicting noise emitted by subsonic jets. The field of Large Eddy Simulation for subsonic jets remains a nascent area with substantial prospects for further exploration and development to enhance our comprehension and modelling capabilities of these intricate flows. Further, real-world subsonic jets encompass diverse physical interactions, including combustion, heat transfer, and acoustics. There is an evident need for research focused on integrating these interactions into the LES model. The difficulty in resolving accurately the near-wall region and capturing small-scale turbulence for complex flow configurations are some additional challenges that lie while using CAA as a cost-effective solution for evaluating jet noise. Addressing these research gaps will enhance the accuracy and reliability of LES predictions for turbulent jets, leading to advancements in various engineering applications, including jet propulsion, environmental impact assessments, and industrial processes.

The hybrid technique employed in this study, when coupled with other physical phenomena, bears the potential to substantially curtail the experimental effort required for parametric studies. Modifications to the geometry could readily facilitate extensive investigations into optimal design configurations for noise control. The imminent challenge lies in streamlining computational costs and time associated with such studies to explore novel noise cancellation mechanisms effectively. In the coming years, the focus will revolve around minimizing these computational constraints, unlocking avenues for probing new realms of noise reduction strategies.

## ACKNOWLEDGMENTS

The authors acknowledge the HPC facility at IIT Gandhinagar. This research was not funded by any grant.

## CONFLICT OF INTEREST

The authors declare no conflicts of interest.

## AUTHORS CONTRIBUTION

K. Tewari (Conceptualization; Formal analysis; Writing - original draft; Writing - review & editing)  
 A. Dewan (Conceptualization; Writing - original draft; Writing - review & editing; Supervision)  
 V. Narayanan (Conceptualization; Writing - original draft; Supervision; Resources)  
 G. Dogra (Formal analysis; Writing - original draft)

## REFERENCES

- [1] ICA Organization, "Carbon offsetting and reduction scheme for international aviation," The International Civil Aviation Organization [Online], 2017. Available: <https://www.icao.int/environmentalprotection/CORSIA/Pages/default.aspx>.
- [2] J. Singh, S. Rana, A. B. A. Hamid, P. Gupta, "Who should hold the baton of aviation sustainability?" *Social Responsibility Journal*, vol. 19, no. 7, pp. 1161–1177, 2022.
- [3] M. Basner, C. Clark, A. Hansell, J. I. Hileman, S. Janssen, K. Shepherd, et al., "Aviation Noise Impacts: State of the Science," vol. 19, no. 87, pp. 41–50, 2017.
- [4] M. Kaltenbach, C. Maschke, R. Klinke, "Health consequences of aircraft noise," *Deutsches Ärzteblatt International*, vol. 105, pp. 548–556, 2008.
- [5] L. Leylekian, M. Lebrun, P. Lempereur, "An overview of aircraft noise reduction technologies," *Aerospace Lab*, vol. 6, pp. 1–15, 2014.
- [6] K. Viswanathan, "Progress in prediction of jet noise and quantification of aircraft/engine noise components," *International Journal of Aeroacoustics*, vol. 17, no. 4–5, pp. 339–379, 2018.
- [7] M. Sadeghian, M. G. Bandpy, "Technologies for aircraft noise reduction: A review," *Journal of Aeronautics & Aerospace Engineering*, vol. 9, no. 1, pp. 1–10, 2020.
- [8] C. K. W. Tam, K. Viswanathan, K. K. Ahuja, J. Panda, "The sources of jet noise: Experimental evidence," *Journal of Fluid Mechanics*, vol. 615, pp. 253–292, 2008.

- [9] T. Suzuki, "A review of diagnostic studies on jet-noise sources and generation mechanisms of subsonically convecting jets," *Fluid Dynamics Research*, vol. 42, no. 1, p. 014001, 2010.
- [10] M. Coderoni, A. S. Lyrintzis, G. A. Blaisdell, "Large-eddy simulations analysis of supersonic heated jets with fluid injection for noise reduction," *AIAA Journal*, vol. 57, no. 8, pp. 3442–3455, 2019.
- [11] H. S. Ribner, "The generation of sound by turbulent jets," *Advances in Applied Mechanics*, vol. 8, pp. 103–182, 1964.
- [12] D. Papamoschou, "New method for jet noise reduction in turbofan engines," *AIAA Journal*, vol. 42, no. 11, pp. 2245–2253, 2004.
- [13] N. K. Depuru-Mohan, M. J. Doty, "Active chevrons for jet noise reduction," in *24th International Congress on Sound and Vibration*, London, Britain, 2017.
- [14] A. Sinha, R. H. Schlinker, J. S. Simonich, R. A. Rebaand T. Colonius, "Toward active control of noise from hot supersonic jets," in *19th AIAA/CEAS Aeroacoustics Conference*, Berlin, Germany, 2013.
- [15] J. J. Choi, A. Annaswamy, O. Egungwu, F. Alvi, "Active noise control of supersonic impinging jet using pulsed microjets," in *43rd AIAA Aerospace Sciences Meeting and Exhibit*, Nevada, United States, 2005.
- [16] M. Azimi, F. Ommi, N. J. Alashti, "Using acoustic liner for fan noise reduction in modern turbofan engines," *International Journal of Aeronautical and Space Sciences*, vol. 15, no. 1, pp. 97–101, 2014.
- [17] P. Balakrishnan, K. Srinivasan, "Pipe jet noise reduction using co-axial swirl pipe," *The Aeronautical Journal*, vol. 121, no. 1238, pp. 488–514, 2017.
- [18] J. Bridges, C. Brown, "Parametric testing of chevrons on single flow hot jets," in *10th AIAA/CEAS Aeroacoustics Conference*, Manchester, Britain, 2004.
- [19] M. Doty, B. Henderson, K. Kinzie, "Turbulent flow field measurements of separate flow round and chevron nozzles with pylon interaction using particle image velocimetry," in *10th AIAA/CEAS Aeroacoustics Conference*, Manchester, Britain, 2004.
- [20] J. Y. He, Y. B. Xu, "Experimental analysis for jet noise reduction of chevron pylon-based nozzles," *Advanced Materials Research*, vol. 1078, pp. 183–186, 2015.
- [21] M. R. O. Gara, J. Bin, N. Sinha, "Optimization of hybrid chevron Lobe nozzle inserts for supersonic jet noise reduction," in *AIAA Aviation Forum*, Texas, United States, 2019.
- [22] G. Cican, M. Deaconu, D.-E. Crunteanu, "Impact of using chevrons nozzle on the acoustics and performances of a micro turbojet engine," *Applied Sciences*, vol. 11, no. 11, p. 5158, 2021.
- [23] A. M. Hanchinal, V. V. Katti, Impingement of coaxial jet on convex element for confined and unconfined flow, *Journal of Mechanical Engineering and Sciences*, vol. 14, no. 2, pp. 6652–6662, 2020.
- [24] K. Tewari, A. Dewan, V. Narayanan, "Computational fluid analysis of flow losses in globe valves," *Fluid Mechanics and Fluid Power*, vol. 1, pp. 19–23, 2021.
- [25] A. H. Ariffin, K. A. Ahmad, "Computational fluid dynamic (CFD) simulation of synthetic jet cooling: A review," *Journal of Advanced Research in Fluid Mechanics and Thermal Sciences*, vol. 72, no. 2, pp. 103–112, 2020.
- [26] Ridwan, M. A. R. Rosnin, A. Aabid, S. A. Khan, J. S. M. Ali, M. A. M. Sapardi, "Effect of expansion level and relief to shear layer in a suddenly expanded flow: A CFD Approach," *Journal of Advanced Research in Fluid Mechanics and Thermal Sciences*, vol. 100, no. 3, pp. 202–229, 2022.
- [27] K. Hakim, H. Toufik, Y. Mouloudj, "Study and simulation of the thrust vectoring in supersonic nozzles," *Journal of Advanced Research in Fluid Mechanics and Thermal Sciences*, vol. 93, no. 1, pp. 13–24, 2022.
- [28] M. J. Lighthill, "On sound generated aerodynamically I. General theory," in *Proceeding of Royal Society A*, vol. 211, no. 1107, pp. 564–587, 1952.
- [29] J. E. F. Williams, D. L. Hawkings, "Sound generation by turbulence and surfaces in arbitrary motion," *Philosophical Transactions for the Royal Society A*, vol. 264, no. 1151, pp. 321–342, 1969.
- [30] M. E. Goldstein, "A generalized acoustic analogy," *Journal of Fluid Mechanics*, vol. 488, pp. 315–333, 2003.
- [31] M. E. Goldstein, "Aeroacoustics of turbulent shear flows," *Annual Review of Fluid Mechanics*, vol. 16, pp. 263–285, 1984.
- [32] S. J. Eastwood, P. G. Tucker, "Hybrid LES—RANS of complex geometry jets," *International Journal of Aeroacoustics*, vol. 10, no. 5/6, pp. 659–684, 2011.

- [33] A. West, M. Caraeni, “Jet noise prediction using a permeable FW-H solver,” in *21st AIAA/CEAS Aeroacoustics Conference*, Texas, United States, 2015.
- [34] D. Lindblad, S. J. Sherwin, C. D. Cantwell, J. Lawrence, A. Proenca, M. Moragues Ginard, “Aeroacoustic analysis of a closely installed chevron nozzle jet using the high-order discontinuous Galerkin method, in *AIAA Aviation Forum*, San Diego, United States, 2023.
- [35] D. J. Bodony, S. K. Lele, “On using large-eddy simulation for the prediction of noise from cold and heated turbulent jets,” *Physics of Fluids*, vol. 17, no. 8, p. 085103, 2005.
- [36] J. C. Tyacke, Z.-N. Wang, P. G. Tucker, “LES–RANS of installed ultra-high-bypass-ratio coaxial jet aeroacoustics with flight stream,” *AIAA Journal*, vol. 57, no. 3, pp. 1215–1236, 2019.
- [37] Y. Jin, X. Han, P. Fan, “Compressibility modified RANS simulations for noise prediction of jet exhausts with chevron,” *Journal of Applied Fluid Mechanics*, vol. 14, pp. 793–804, 2020.
- [38] G. A. Brès, S. K. Lele, “Modelling of jet noise: a perspective from large-eddy simulations,” *Philosophical Transactions of the Royal Society A*, vol. 377, p. 20190081, 2019.
- [39] R. R. Mankbadi, “Review of computational aeroacoustics in propulsion systems,” *Journal of Propulsion Power*, vol. 15, no. 4, pp. 504–512, 1999.
- [40] P. Jordan, Y. Gervais, J. C. Valière, H. Foulon, “Final results from single point LDV measurements. Project deliverable D3.4, JEAN – EU Framework Programme, G4RD-CT-2000-00313, *Laboratoire d’Etude Aerodynamiques*, 2002
- [41] A. N. Secundov, S. F. Birch, P. G. Tucker, “Propulsive jets and their acoustics,” *Philosophical Transactions of the Royal Society A*, vol. 365, pp. 2443–2467, 2007.
- [42] A. Uzun, M. Y. Hussaini, “Investigation of high frequency noise generation in the near-nozzle region of a jet using large eddy simulation,” *Theoretical and Computation Fluid Dynamics*, vol. 21, pp. 291–321, 2007.
- [43] U. Piomelli, J. R. Chasnov, “Large-eddy simulations: Theory and applications,” *Turbulence and Transition Modelling*, vol. 2, pp. 269–336, 1996.
- [44] A. Dewan, *Tackling Turbulent Flows in Engineering*. 1st Ed. Berlin, Germany: Springer Berlin Heidelberg, 2010.
- [45] C. Seror, P. Sagaut, C. Bailly, D. Juvé, “On the radiated noise computed by large-eddy simulation,” *Physics of Fluids*, vol. 13, pp. 476–487, 2001.
- [46] A. K. Shukla, A. Dewan, “OpenFOAM based LES of slot jet impingement heat transfer at low nozzle to plate spacing using four SGS models,” *Heat and Mass Transfer*, vol. 55, pp. 911–931, 2019.
- [47] A. K. Shukla, A. Dewan, “Flow and thermal characteristics of jet impingement on a flat plate for small nozzle to plate spacing using LES,” *International Journal of Thermal Sciences*, vol. 145, p. 106005, 2019.
- [48] C. Meneveau, J. Katz, “Scale-invariance and turbulence models for large-eddy simulation,” *Annual Review of Fluid Mechanics*, vol. 32, pp. 1–32, 2000.
- [49] M. Shur, P. Spalart, M. Strelets, A. Garbaruk, “Further steps in LES-based noise prediction for complex jets,” in *44th AIAA Aerospace Sciences Meeting and Exhibit*, Nevada, United States, 2006.
- [50] N. Andersson, L.-E. Eriksson, L. Davidson, “Investigation of an isothermal Mach 0.75 jet and its radiated sound using large-eddy simulation and Kirchhoff surface integration,” *International Journal of Heat and Fluid Flow*, vol. 26, no. 3, pp. 393–410, 2005.
- [51] P. S. Tide, V. Babu, “Numerical predictions of noise due to subsonic jets from nozzles with and without chevrons,” *Applied Acoustics*, vol. 70, no. 2, pp. 321–332, 2009.
- [52] C. Brown, J. Bridges, “Acoustic efficiency of azimuthal modes in jet noise using chevron nozzles,” in *12th AIAA/CEAS Aeroacoustics Conference*, Massachusetts, United States, 2006.

## NOMENCLATURE

### Abbreviations

CAA	Computational Aero Acoustics	LES	Large Eddy Simulations
CFD	Computational Fluid Dynamics	NIH	Noise Induced Hearing Loss
DNS	Direct Numerical Simulation	OASPL	Overall Sound Pressure Levels
FW-H	Ffowcs Williams Hawkings	RANS	Reynolds Averaged Navier Stokes
JEAN	Jet Exhaust Aerodynamic Noise	SPL	Sound Pressure Level